Journal of Sound and Vibration 329 (2010) 1536–1552

Contents lists available at ScienceDirect

Journal of Sound and Vibration

journal homepage: www.elsevier.com/locate/jsvi

Vibration analysis of horizontal self-weighted beams and cables with bending stiffness subjected to thermal loads

Fabien Treyssède *

Laboratoire Central des Ponts et Chaussées, BP 4129, 44341 Bouguenais, France

ARTICLE INFO

Article history:
Received 24 July 2009
Received in revised form
13 November 2009
Accepted 13 November 2009
Handling Editor: L.N. Virgin
Available online 11 December 2009

ABSTRACT

This paper aims at proposing an analytical model for the vibration analysis of horizontal beams that are self-weighted and thermally stressed. Geometrical nonlinearities are taken into account on the basis of large displacement and small rotation. Natural frequencies are obtained from a linearization of equilibrium equations. Thermal force and thermal bending moment are both included in the analysis. Torsional and axial springs are considered at beam ends, allowing various boundary conditions. A dimensionless analysis is performed leading to only four parameters, respectively, related to the self-weight, thermal force, thermal bending moment and torsional spring stiffness. It is shown that the proposed model can be efficiently used for cable problems with small sag-to-span ratios (typically $< \frac{1}{8}$, as in Irvine's theory). For beam problems, the model is validated thanks to finite element solutions and a parametric study is conducted in order to highlight the combined effects of thermal loads and self-weight on natural frequencies. For cable problems, solutions are first compared with existing results in the literature obtained without thermal effects or bending stiffness. Good agreement is found. A parametric study combining the effects of sag-extensibility, thermal change and bending stiffness is finally given.

1. Introduction

Beams and cables are widely used in civil structures. Such structures are subjected to various external forces. Among them, self-weight and environmental thermal loads are inevitable. These quasi-static loads yield initial stress (prestress) and initial displacement (predisplacement) affecting the dynamical behaviour of structures. For thin structures such as beams, the effect of prestress is enhanced by the slenderness ratio, so that even low prestressed states far from the buckling stage may have a significant impact on dynamics.

Modal vibration analyses of beams subjected to purely axial prestress have received much attention in the literature—see Refs. [1,2] for instance. It is well-known that the natural frequencies of flexural vibration increase (resp. decrease) when the axial load is tensile (resp. compressive) and that this effect is stronger for lower eigenfrequencies. The effect of axial thermal stress on modal parameters has naturally been included, particularly recently with the emergence of composite or functionally graded beams [3–6]. For self-weighted vertical beams, the load is also purely axial, though non-constant, and some linear analyses can be found in Refs. [7–10].

However, geometrical nonlinearities are often neglected in prestressed modal analyses. From the point of view of small superimposed vibrations, geometrical nonlinearities are regarded as predisplacements, generally related to prebending.

* Tel.: +33 240845932; fax: +33 240845998.
E-mail address: fabien.treyssede@lcpc.fr

0022-460X/$ - see front matter © 2009 Elsevier Ltd. All rights reserved.
doi:10.1016/j.jsv.2009.11.018

In practice, bending naturally occurs for large self-weighted beams, thermally prestressed inhomogeneous structures (thickness varying, composite, functionally graded,…), beams subjected to temperature gradients along their thickness, non-straight beams,…In static buckling analyses, the non-negligible effect of initial displacement is rather well-known. It is yet barely considered in modal vibration analyses, although early works have analytically and experimentally demonstrated the potential effect of initial bending upon vibrations [11–15]. More recent studies can be found in Refs. [16–19] for instance, and the reader can refer to Refs. [20–23] for extensions to thermoelasticity. Small vibrations of self-weighted vertical beams around post-buckled states have recently been analysed in Ref. [24]. To the author's knowledge, the vibration analysis of horizontal beams that are naturally prebended under self-weight has not been explicitly investigated in the literature—if one excepts cables.

The mechanics of cables can be considered as a particular case of beams. As a first approximation, a cable can be viewed as a geometrically nonlinear beam having no bending stiffness, subjected to self-weight and an externally applied force. The literature on cable dynamics is large (a review is beyond the scope of this paper), Irvine's work [25] being one of the most important contributions. Irvine showed that only one dimensionless parameter is needed to determine natural frequencies of cables. Recent studies have aimed at taking into account bending stiffness [26–28], which can be significant for the prediction of higher order modes or large diameter cables. However, the investigation of thermal effects on cable dynamics has surprisingly not received a great attention in the literature. Only recently, Treyssede [29] extended Irvine's model to thermoelasticity.

The goal of this paper is to investigate the effects of temperature on the modal behaviour of horizontal beams taking into account self-weight, as well as cables taking into account bending stiffness. It is focused on moderate loads yielding prebuckled configurations (though the approach remains valid for post-buckled cases). Only small vibrations are considered, which is a necessary assumption for performing a modal analysis in the classical sense (nonlinear vibrations are beyond the scope of this paper). In Section 2, an analytic and dimensionless solution is derived for the statics and dynamics of an initially horizontal beam subjected to self-weight, thermal force and thermal bending moment. Torsional and axial springs are considered at beam ends, which allows various boundary conditions. Dimensionless parameters are highlighted. The solution is valid both for negative and positive thermal changes (tensile and compressive loads). It also shown that the proposed model also applies for cables thanks to the calculation of an equivalent thermal parameter for the cable tension. In Section 3, results obtained for beam and cable problems are presented and considered independently for clarity. For beam problems, the model is validated thanks to finite element (FE) solutions and a parametric study is conducted in order to highlight the combined effects of thermal loads and self-weight on natural frequencies. For cable problems, solutions are first compared with existing results in the literature obtained without thermal effects or bending stiffness. A parametric study combining the effects of sag-extensibility, thermal change and bending stiffness is finally given.

One of the motivations of this study is the potential need of adequate models for vibration based methods in structural health monitoring (SHM). These methods are potentially attractive for damage detection in civil structures [30–35] or tension estimation [36–38]. However, they are likely to suffer a lack of robustness because of environmental temperature change (affecting the prestress state and in turn its modal parameters). It is well-known that differentiating changes due to the environment from changes due to damage is still a challenging task [39–41]. Typical applications in civil engineering are bridges and buildings subjected to climatic thermal variations: for such structures, the daily variation of natural frequency may reach several percent [42,43]. In addition to SHM, one could also note that temperature changes may also affect the robustness of vibration control strategies [44–46].

2. Model

2.1. Assumptions and notations

Here are the beam assumptions adopted throughout the paper:

- the beam is initially perfectly straight (no imperfection) and has a horizontal neutral axis, denoted x;
- the strain–displacement relationship is based on the Von Karman approximation (nonlinear terms involving the axial displacement are neglected), which is generally valid for small strains, large displacements, small rotations;
- the shear strain is neglected (Euler–Bernoulli kinematics);
- the material is linearly elastic;
- the axial and rotary inertia are neglected; and
- all beam characteristics are uniform along x (material properties, temperature,…).

The only type of nonlinearity is hence geometrical. In prestressed dynamics, three states must be distinguished: the reference state (unprestressed), the intermediate state (prestressed), and the current state (perturbed by superimposed dynamics). Fig. 1 depicts the beam profile for its three equilibrium configurations. Equilibrium equations of this paper are based on a total Lagrangian approach, which means that x represents the position of a material point in its reference configuration. The present study is restricted to static prestressed states and small linear dynamic perturbations.

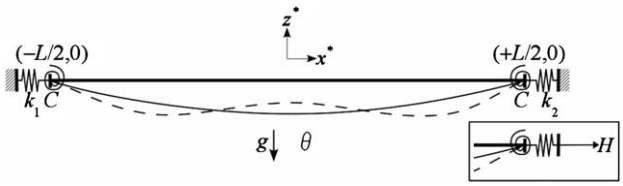

Fig. 1. Beam boundary conditions, loads and profiles for the reference state (thick line), the prestressed state (thin line) and the dynamic state (dashed line). The prestressed state is under the action of self-weight and thermal loads. The dynamic profile here corresponds to a second symmetric in-plane mode. Inset: cable boundary conditions (a tensile horizontal force H is applied at the end of the spring instead of a zero axial displacement).

Quantities referring to the intermediate and current states will, respectively, be denoted with a subscript 0 and a tilde. The absence of symbol will be left for dynamic perturbations. For clarity, w_0 and N_0 will denote the beam transverse predisplacement (vertical) and the axial pretension, while $\tilde{w}$ and $\tilde{N}$ will be the total displacement and tension. $w=\tilde{w}-w_0$ and $N=\tilde{N}-N_0$ will be the corresponding vibrating perturbations.

Note that the Von Karman hypothesis restricts the proposed model to prestressed states for which the static predeflection w_0 and pretension N_0 are not too large. As discussed in Section 3.1.2, the validity of the dimensionless results presented in this paper indeed depends on the value of the slenderness ratio of the considered structure.

Variables are made dimensionless, with the following choice:

$$\tilde{w}=\tilde{w}^*/r, \quad \tilde{N}=\tilde{N}^*L^2/EI, \quad x=x^*/L, \quad t=t^*/t_c \tag{1}$$

The asterisk is used to designate dimensional variables. L is the length of the beam. r is the radius of gyration, defined by $r^2=I/A$. The characteristic time t_c will be chosen as $t_c^2=\rho AL^4/EI$. E, ρ, α, A, I and g, respectively, denote the Young's modulus, material density, thermal expansion coefficient, cross-section area, second moment of inertia and constant of gravity. k_1 and k_2 will denote the stiffness of translational axial springs (in N m $^{-1}$) and C will be the stiffness of torsional springs (in N m), located at beams ends $x^*=\pm L/2$. N_T and M_T denote the thermal force and thermal bending moment, defined as

$$(N_T,M_T)=\int_A E\alpha\theta(1,z^*)\,\mathrm{d}A \tag{2}$$

where $\theta=T-T_{\mathrm{ref}}$ is the temperature change, T_{ref} being the reference temperature (beam at complete rest). z^* is the dimensional transverse direction of the beam. For clarity, Appendix A gives a brief note on heat transfer and related assumptions that may or may not be applied for the analysis of civil structures.

2.2. Equilibrium equations

For conciseness, no detail is given on the derivation of beam thermoelastic equilibrium equations, which can be found elsewhere in the literature—see [47,22,48] for instance. Based on the previously mentioned assumptions and dimensionless variables given by Eqs. (1) it can be shown that the equations governing the equilibrium of current state are

$$\frac{\mathrm{d}^4\tilde{w}}{\mathrm{d}x^4}-\tilde{N}\frac{\mathrm{d}^2\tilde{w}}{\mathrm{d}x^2}+\ddot{\tilde{w}}=-\gamma \tag{3}$$

with the axial tension given by

$$\tilde{N}=\frac{1}{1+f}\left\{\frac{1}{2}\int_{-1/2}^{+1/2}\left(\frac{\mathrm{d}\tilde{w}}{\mathrm{d}x}\right)^2\mathrm{d}x-\mu_0\right\} \tag{4}$$

and the boundary conditions, chosen as follows:

$$\tilde{w}\big|_{\pm 1/2}=0, \quad \frac{\mathrm{d}^2\tilde{w}}{\mathrm{d}x^2}\pm\kappa\frac{\mathrm{d}\tilde{w}}{\mathrm{d}x}\bigg|_{\pm 1/2}=-\mu_1 \tag{5}$$

The dimensionless parameters, appearing in Eqs. (3)–(5), are

$$\gamma=\frac{\rho gL}{E}\sigma^3, \quad \mu_0=\frac{N_T}{EA}\sigma^2, \quad \mu_1=\frac{M_T}{EAr}\sigma^2, \quad f=\frac{EA}{L}\left(\frac{1}{k_1}+\frac{1}{k_2}\right), \quad \kappa=\frac{C}{EAr}\sigma \tag{6}$$

where $\sigma=L/r$ is the slenderness ratio. γ, μ_0 and μ_1 are load parameters, respectively, related to the self-weight, thermal force and thermal bending moment. As can be noticed, their effects are all enhanced by the slenderness ratio (thinner beams will hence be quite sensitive to a prestressed state). f represents a dimensionless equivalent flexibility due to the presence of translational axial springs. $f=0$ when k_1 and k_2 tends to infinity (zero axial displacement at ends). κ is a parameter quantifying the effect of torsional springs. Perfectly hinged and clamped boundary conditions can be obtained by setting $\kappa=0$ and $\kappa\to\infty$, respectively.

The fact that the tension $\tilde{N}$ remains axially constant (positive when tensile, negative when compressive), as shown by Eq. (4), is due to the assumption of neglecting axial inertia. As a side remark, it could be checked that parameters

quantifying the effects of axial and rotary inertia are given by $1/\sigma$ and $1/\sigma^2$, respectively. Then, it is worthy to note that neglecting their effects as done in this paper is only possible for high enough slenderness ratio.

From Eqs. (3)–(6), it can be deduced that:

- at equal slenderness ratio, the effect of γ increases for longer structures (the dynamics of large civil structures is thus more likely to be affected by self-weight);
- when $f \gg 1$ ($k_1, k_2 \to 0$), $\tilde{N}$ tends to zero (the effect of thermal force becomes negligible for axially free beams); and
- for $\kappa \gg \mu_1$, the effect of μ_1 becomes negligible (clamped beams are not affected by thermal bending).

2.3. Static prestressed state

For static prestressed states, the equilibrium equations become:

$$\begin{cases} \dfrac{\mathrm{d}^4 w_0}{\mathrm{d}x^4} - N_0 \dfrac{\mathrm{d}^2 w_0}{\mathrm{d}x^2} = -\gamma \\ N_0 = \dfrac{1}{1+f}\left\{ \dfrac{1}{2}\int_{-1/2}^{+1/2} \left(\dfrac{\mathrm{d}w_0}{\mathrm{d}x}\right)^2 \mathrm{d}x - \mu_0 \right\} \\ w_0|_{\pm 1/2} = 0 \\ \left.\dfrac{\mathrm{d}^2 w_0}{\mathrm{d}x^2} \pm \kappa \dfrac{\mathrm{d}w_0}{\mathrm{d}x}\right|_{\pm 1/2} = -\mu_1 \end{cases} \tag{7}$$

Taking into account that N_0 is a constant (to be determined) and the symmetry of the problem ($\mathrm{d}w_0/\mathrm{d}x = \mathrm{d}^3 w_0/\mathrm{d}x^3 = 0$ at $x = 0$), it can be shown that a general solution of the differential equation of system (7) can be given by

$$w_0(x) = A_0 + B_0 \cosh\sqrt{N_0}x + \frac{\gamma}{N_0}\left(\frac{x^2}{2} - \frac{1}{8}\right) \tag{8}$$

where A_0 and B_0 are constants. Applying boundary conditions at $x = \frac{1}{2}$ yields

$$B_0 = -\frac{\dfrac{\gamma}{N_0}\left(1+\dfrac{\kappa}{2}\right) + \mu_1}{N_0 \cosh\dfrac{\sqrt{N_0}}{2} + \kappa\sqrt{N_0}\sinh\dfrac{\sqrt{N_0}}{2}} \tag{9}$$

and $A_0 = -B_0 \cosh\sqrt{N_0}/2$.

Then, substituting Eq. (8) into the expression for N_0 in system (7) gives

$$N_0 + \frac{\mu_0}{1+f} + \frac{B_0^2 N_0}{4(1+f)}\left(1 - \frac{\sinh\sqrt{N_0}}{\sqrt{N_0}}\right) - \frac{\gamma B_0}{(1+f)N_0}\left(\cosh\frac{\sqrt{N_0}}{2} - 2\frac{\sinh\frac{\sqrt{N_0}}{2}}{\sqrt{N_0}}\right) - \frac{\gamma^2}{24(1+f)N_0^2} = 0 \tag{10}$$

Provided that B_0 is written in terms of N_0, as given by Eq. (9), the solution of the above equation allows to determine the axial tension N_0. This equation must be numerically solved (a Newton–Raphson algorithm is used in this paper). It is emphasized that the solution given by Eqs. (8)–(10) remains valid for $N_0 < 0$ also, thanks to the formula: $\sqrt{y} = \mathrm{i}\sqrt{-y}$ for $y \leqslant 0$, $\cosh \mathrm{i}y = \cos y$ and $\sinh \mathrm{i}y = \mathrm{i}\sin y$. Note that the last term in Eq. (8) corresponds to the standard cable solution (parabolic profile) [25], which is recovered when N_0 is high enough.

A fundamental result is obtained from a further inspection of Eq. (10), which shows that N_0 can indeed be determined from the following four dimensionless parameters (instead of five):

$$\frac{\gamma^2}{1+f}, \quad \frac{\mu_0}{1+f}, \quad \frac{\mu_1}{\sqrt{1+f}}, \quad \kappa \tag{11}$$

2.4. Prestressed dynamics

The equations governing the equilibrium of superimposed dynamics are obtained from a direct linearization of Eqs. (3)–(5), which yields the following eigenproblem:

$$\begin{cases} \dfrac{\mathrm{d}^4 w}{\mathrm{d}x^4} - N_0 \dfrac{\mathrm{d}^2 w}{\mathrm{d}x^2} - \Omega^2 w = N \dfrac{\mathrm{d}^2 w_0}{\mathrm{d}x^2} \\ N = \dfrac{1}{1+f}\displaystyle\int_{-1/2}^{+1/2} \dfrac{\mathrm{d}w_0}{\mathrm{d}x}\dfrac{\mathrm{d}w}{\mathrm{d}x}\mathrm{d}x \\ w|_{\pm 1/2} = 0 \\ \left.\dfrac{\mathrm{d}^2 w}{\mathrm{d}x^2} \pm \kappa \dfrac{\mathrm{d}w}{\mathrm{d}x}\right|_{\pm 1/2} = 0 \end{cases} \tag{12}$$

where an $\mathrm{e}^{-\mathrm{i}\Omega t}$ time harmonic dependence has been assumed, $\Omega = \omega t_c$ being the dimensionless angular frequency.

From a vibrational point of view, the prestressed state acts upon dynamics through the couple (N_0, w_0) (axial pretension, transverse predisplacement). Note that $f \gg 1$ yields $N, N_0 \to 0$, which means that the dynamics of an axially free beam is not sensitive to the prestressed state.

2.4.1. Antisymmetric modes

Antisymmetric modes verify the conditions $w = \mathrm{d}^2w/\mathrm{d}x^2 = 0$ at $x = 0$. Because $\mathrm{d}w_0/\mathrm{d}x$ is antisymmetric, such modes have a zero dynamic tension $N = 0$. Then, the general solution of the differential equation in system (12) is simply:

$$w^a(x) = A\sin\lambda_- x + B\sinh\lambda_+ x \tag{13}$$

with the notation:

$$\lambda_\pm = \sqrt{\frac{\sqrt{N_0^2 + 4\Omega^2} \pm N_0}{2}} \tag{14}$$

The superscript a (resp. s) will be used for denoting antisymmetric (resp. symmetric) modes. Applying boundary conditions at $x = \frac{1}{2}$ to Eq. (13) gives a two-by-two system for A and B, whose zero determinant is

$$\sin\frac{\lambda_-}{2}\sinh\frac{\lambda_+}{2}(\lambda_-^2 + \lambda_+^2) + \kappa\left(\lambda_+\sin\frac{\lambda_-}{2}\cosh\frac{\lambda_+}{2} - \lambda_-\cos\frac{\lambda_-}{2}\sinh\frac{\lambda_+}{2}\right) = 0 \tag{15}$$

This transcendental equation can be numerically solved and admits an infinity of eigenfrequencies Ω_n^a $(n = 1, \ldots, \infty)$. The only influence of the prestressed state on antisymmetric modes is the axial pretension N_0. N_0 and κ are hence the only independent parameters for determining antisymmetric eigenmodes.

2.4.2. Symmetric modes

The boundary conditions for symmetric modes are $\mathrm{d}w/\mathrm{d}x = \mathrm{d}^3w/\mathrm{d}x^3 = 0$ at $x = 0$. Their axial dynamic tension N is non-zero. In the differential equation of system (12), both terms in N_0 and w_0 are non-zero. Adding the homogeneous solution to a particular one, it can be checked that a general symmetric solution is:

$$w^s(x) = A\cos\lambda_- x + B\cosh\lambda_+ x - \frac{N}{\Omega^2}\left(\frac{\gamma}{N_0} + B_0N_0\cosh\sqrt{N_0}x\right) \tag{16}$$

One must now determine N with respect to A and B. This can be done from the expression of N in system (12) and using Eqs. (8) and (16). After tedious calculations, one gets the linear relationship:

$$N = \alpha_-\Omega^2 A + \alpha_+\Omega^2 B \tag{17}$$

where the expressions of α_- and α_+ are given in Appendix B. Then, applying the boundary conditions at $x = \frac{1}{2}$ to the expression (16) yields the following homogeneous system for A and B:

$$\begin{bmatrix} a_{11} & a_{12} \\ a_{21} & a_{22} \end{bmatrix}\begin{Bmatrix} A \\ B \end{Bmatrix} = \begin{Bmatrix} 0 \\ 0 \end{Bmatrix} \tag{18}$$

whose coefficients are

$$a_{11} = \cos\frac{\lambda_-}{2} - \alpha_-\left(\frac{\gamma}{N_0} + B_0N_0\cosh\frac{\sqrt{N_0}}{2}\right)$$

$$a_{12} = \cosh\frac{\lambda_+}{2} - \alpha_+\left(\frac{\gamma}{N_0} + B_0N_0\cosh\frac{\sqrt{N_0}}{2}\right)$$

$$a_{21} = -\lambda_-^2\cos\frac{\lambda_-}{2} - \kappa\lambda_-\sin\frac{\lambda_-}{2} - \alpha_-B_0N_0^2\left(\cosh\frac{\sqrt{N_0}}{2} + \kappa\frac{\sinh\frac{\sqrt{N_0}}{2}}{\sqrt{N_0}}\right)$$

$$a_{22} = \lambda_+^2\cosh\frac{\lambda_+}{2} + \kappa\lambda_+\sinh\frac{\lambda_+}{2} - \alpha_+B_0N_0^2\left(\cosh\frac{\sqrt{N_0}}{2} + \kappa\frac{\sinh\frac{\sqrt{N_0}}{2}}{\sqrt{N_0}}\right) \tag{19}$$

The transcendental equation for Ω is given by a zero determinant: $a_{11}a_{22} - a_{12}a_{21} = 0$. Its numerical solutions are the symmetric eigenfrequencies Ω_n^s $(n = 1, \ldots, \infty)$. As for Section 2.3, all expressions remain valid for $N_0 < 0$. The inspection of Eqs. (19) shows that the independent parameters for the determination of the Ω_n^s are the same as the ones given by Eq. (11).

2.5. Cable-like problems

The solution can be readily modified in order to treat cable-like problems, for which an initial positive horizontal force H (in Newton) is prescribed at one end of the beam (see inset of Fig. 1). The dimensionless parameter associated to the applied force is denoted ξ^2 and given by

$$\xi^2 = HL^2/EI \tag{20}$$

ξ^2 is indeed equal to a dimensionless force N_0 corresponding to a prestressed state with no thermal load but self-weight. Replacing N_0 with ξ^2 into the solutions derived in Sections 2.3 and 2.4 yields valid cable solutions with no thermal effect but bending stiffness, as checked in Section 3.2.1.

From Eq. (10), the equivalent thermal force parameter to the applied force, denoted $\mu_{0_{\mathrm{eq}}}$, is given by

$$\mu_{0_{\mathrm{eq}}} = -(1+f)\xi^2 - \frac{B_{0_{\mathrm{eq}}}^2\xi^2}{4}\left(1-\frac{\sinh\xi}{\xi}\right) + \frac{\gamma B_{0_{\mathrm{eq}}}}{\xi^2}\left(\cosh\frac{\xi}{2} - 2\frac{\sinh\frac{\xi}{2}}{\xi}\right) + \frac{\gamma^2}{24\xi^4} \tag{21}$$

where

$$B_{0_{eq}} = -\frac{\frac{\gamma}{\xi^2}\left(1+\frac{\kappa}{2}\right)}{\xi^2\cosh\frac{\xi}{2} + \kappa\xi\sinh\frac{\xi}{2}} \tag{22}$$

The modified axial force caused by thermal change is then given by the solution N_0 of Eq. (10) obtained by replacing μ_0 with $\mu_{0_{\mathrm{eq}}} + \mu_0$.

Without bending stiffness, the standard cable parameters are the Irvine sag-extensibility parameter λ^2 and the thermal parameter θ, whose expressions can be found in Refs. [25,29]. When the bending stiffness is taken into account, a third dimensionless parameter ξ is also considered. ξ is often referred to as the bending stiffness parameter [25,27], measuring the relative importance of cable and beam action (when ξ is small, beam action predominates, while cable action is predominant when ξ is large).

Noticing that $\rho AgL/H = \gamma/\sigma\xi^2$, λ^2 and θ can be expressed in terms of dimensionless parameters found in this paper, namely $\gamma^2/1+f$, $\mu_0/1+f$ and ξ, as follows:

$$\lambda^2 = \frac{\gamma^2}{\xi^6(1+f)}\left(1+\frac{\gamma^2}{8\sigma^2\xi^4(1+f)}\right)^{-1}, \quad \theta = \frac{\mu_0}{\xi^2(1+f)}\left(1+\frac{\gamma^2}{12\sigma^2\xi^4}\right)\left(1+\frac{\gamma^2}{8\sigma^2\xi^4(1+f)}\right)^{-1} \tag{23}$$

A new parameter $\gamma/\sigma\xi^2$ appears in the above expressions. This parameter is related to the sag-to-span ratio (in Irvine's model, the sag-to-span ratio is $\rho AgL/8H = \gamma/8\sigma\xi^2$). What must be understood is that the sag-to-span ratio is also needed, in addition to the usual parameters (λ^2, θ, ξ), for a precise characterization of cables with bending stiffness (as considered in this paper). This conclusion coincides with the parametric study of Ni et al. [27], who considered different cable sets having the same range of λ^2 and ξ, but different range of sag-to-span ratio.

Note that Irvine's model is only valid for small sag-to-span ratio, typically $< \frac{1}{8}$, which implies that $\gamma/\sigma\xi^2 \leqslant 1$ (the model proposed in this paper is also valid for small-sag-span ratio because of the assumption of small rotation). The influence of $\gamma/\sigma\xi^2$ on λ^2 and θ is hence limited. In this paper, the following modified cable parameters are proposed instead:

$$\lambda'^2 = \frac{\gamma^2}{\xi^6(1+f)}, \quad \theta' = \frac{\mu_0}{\xi^2(1+f)} \tag{24}$$

so that the number of dimensionless parameters governing the problem, now given by $(\lambda'^2, \theta', \xi)$, is truly reduced to three. Also, the dimensionless frequency $\Omega' = \Omega/\xi$ will be used, as chosen in Irvine's theory.

3. Results

Provided that one is interested in relatively low temperature change due to climatic variations, the influence of temperature on material properties is neglected in the following results (without loss of generality).

3.1. Beams

In this subsection, beam ends are held fixed with no applied force, so that the axial tension N_0 only results from the action of self-weight. Solutions are obtained from a Newton–Raphson algorithm. At fixed γ, μ_0 is gradually increased and a linear extrapolation is used for the initial guess of the next solution. N_0 then gradually decreases: if the buckling temperature is reached, several solutions may exist for N_0 (post-buckling regimes) and the lowest $|N_0|$ is automatically selected.

3.1.1. FE validation

Fig. 2 exhibits the evolution of the first dimensionless frequency Ω for $\gamma = 15$ and a temperature change μ_0 varying from -20 to $+20$ ($f = \kappa = \mu_1 = 0$). This first test case corresponds to a simply supported beam having the following dimensional characteristics: $L = 1$ m, $r = 0.0029$ m, $E = 2.0\text{e}{+11}$ Pa, $\rho = 7800\,\text{kg m}^{-3}$, $\alpha = 1.2\text{e}{-5}\,\text{K}^{-1}$, $g = 9.81\,\text{m s}^{-2}$, and θ varying from -14.4 to $+14.4$ K. If the self-weight is neglected ($\gamma = 0$), the beam remains straight (no prebending) and the following analytical solution can be obtained for the n th natural frequency:

$$\Omega_n = n\pi\sqrt{n^2\pi^2 - \mu_0} \tag{25}$$

This solution is also plotted in Fig. 2 for the first frequency, which clearly shows that for $\mu_0 \geq \pi^2$ (π^2 being the critical thermal force), the beam buckles and the 1st mode vanishes. However, if the self-weight is taken into account ($\gamma = 15$), the frequency then increases. This is due to the fact that the beam is prebent under the action of self-weight, which causes an increase of curvature and plays the same role as initial imperfections [14] or thermal moments [20]. These results are in good agreement with FE solutions obtained from an Euler–Bernoulli planar beam model, already presented in Ref. [22] (this FE model is thermoelastic and takes into account geometrical nonlinearities).

Fig. 3 exhibits the evolution of the first dimensionless frequency Ω for $\gamma = 300$ and a temperature change μ_0 varying from -12 to $+12$ ($f = \kappa = 0$). This second test case corresponds to a large simply supported beam having the same

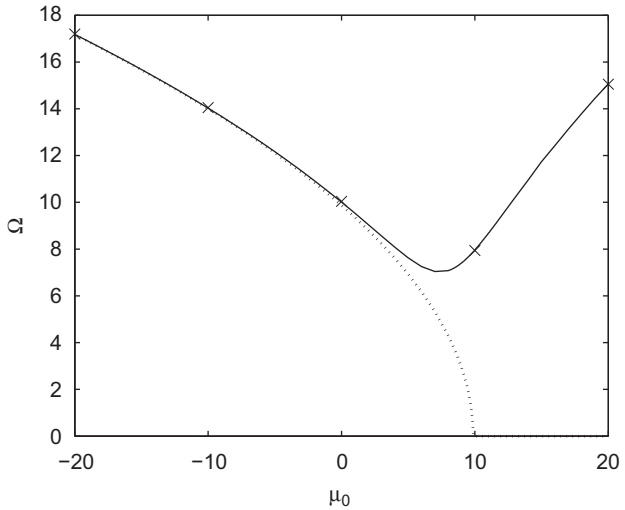

Fig. 2. Dimensionless 1st frequency vs. temperature change for $\gamma = 15$ ($f = \kappa = \mu_1 = 0$). Continuous line: proposed model, dotted line: analytical solution for $\gamma = 0$, x-mark: FE solution.

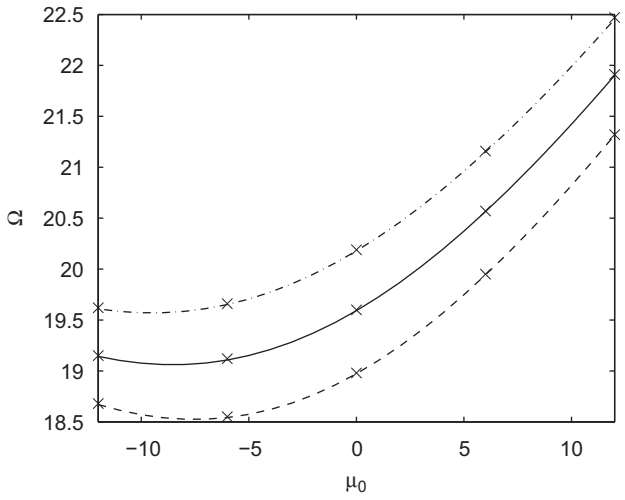

Fig. 3. Dimensionless 1st frequency vs. temperature change for $\gamma = 300$ ($f = \kappa = 0$). Black line: $\mu_1 = 0$, dashed: $\mu_1 = +2.5$, dashed dotted: $\mu_1 = -2.5$, x-mark: FE solution.

characteristics as before, except that $L=200\,\mathrm{m}$, $r=1.2684\,\mathrm{m}$, and θ varies from -40 to $+40\,\mathrm{K}$. The cross-section is a $3\times 12\,\mathrm{m}$ rectangular box of 0.3 m thickness. A linear temperature distribution is assumed across the depth of the cross-section, yielding a thermal bending moment. Three values of μ_1 are considered: -2.5, 0, $+2.5$, respectively, corresponding to a temperature difference between the top and the bottom of -19.8, 0 and $+19.8\,\mathrm{K}$ (such temperature gradients may exist in bridge decks [49–51]). As observed, the frequency changes nonlinearly and non-monotically with μ_0. The presence of a thermal gradient on the cross-section yields non-negligible differences. A positive gradient (temperature higher on the top) yields a positive deflection that compensates the self-weight deflection, explaining a decrease of frequency. Inversely, a negative gradient tends to enhance the deflection, and hence increases the frequency. Also shown in Fig. 3 are FE results obtained with the code developed in Ref. [22]. Good agreement is found, which validates the proposed analytical model for beams.

3.1.2. *Parametric study*

Let us consider the case $\kappa=\mu_1=0$ (simple supports, no thermal bending moment). From Eq. (11), the only independent parameters of the problem are $\gamma^2/(1+f)$ and $\mu_0/(1+f)$, so that quite general results can be obtained through two-dimensional contour plots. A parametric study is briefly reported. Due to large range of variations and for a better clarity of figures, the axes of contour plots are chosen as $(\gamma^2/(1+f))^{1/4}$ and $|\mu_0/(1+f)|^{1/2}\mathrm{sgn}\mu_0$.

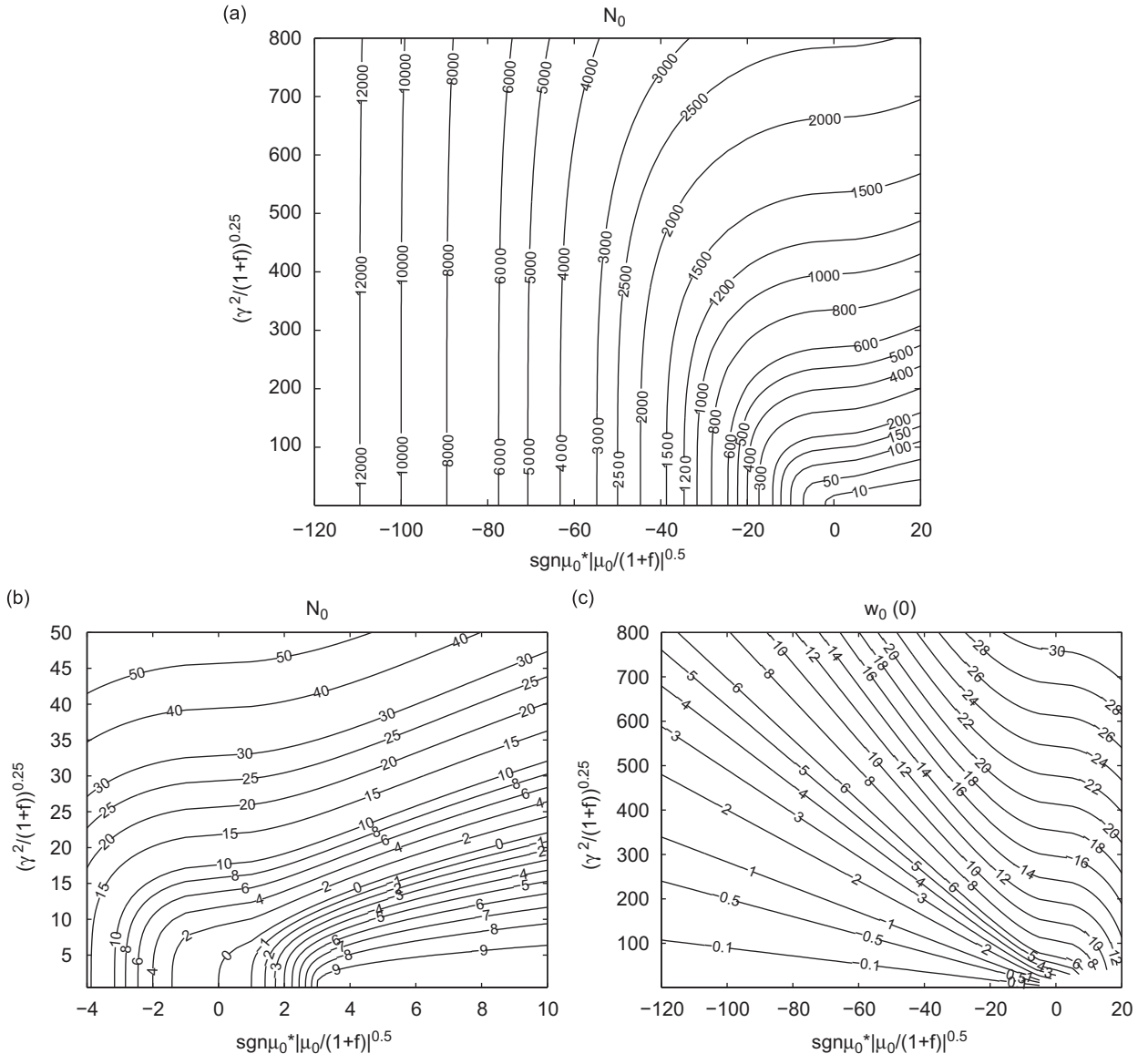

Fig. 4. Contour plots of N_0 (a)-(b) and $w_0(0)$ (c) for $f=\kappa=\mu_1=0$.

Fig. 4 exhibits the axial force N_0 and the predisplacement at centre $w_0(0)$. One focuses on prebuckling regimes and results are not shown for $N_0 \leqslant -\pi^2$ (note that the predisplacement $w_0(0)$ remains negative). As expected, N_0 and $|w_0(0)|$ increase as the self-weight parameter increases, N_0 and $w_0(0)$ decrease as the thermal force parameter increases (heating). Due to the assumption of small rotation and small strain, it should be noted that the validity of the proposed model is limited to small values of $w_0^*(0)/L = w_0(0)/\sigma$ and $N_0^*/EA = N_0/\sigma^2$ (the validity of solutions hence depends on σ).

As far as contour plots are concerned in this subsection, the variation range of γ and μ_0 has been chosen in order to treat a wider range of problems, from strings to beams including cables. The beam-like zone is concentrated on the lower part near the origin, where N_0 is rather low (which means that the bending stiffness cannot be neglected). The cable-like zone roughly corresponds to the right upper part of plots, where N_0 is high enough for neglecting bending stiffness effects but where $w_0(0)/\sigma$ (sag-to-span ratio) becomes non-negligible. Natural frequencies of strings, which are given by $\Omega_n = n\pi\sqrt{N_0}$, can be recovered for sufficiently high N_0 (negligible bending stiffness) and small $|w_0/\sigma|$ (negligible sag): this zone typically corresponds to the left-hand part of contour plots, where contours becomes vertical lines.

Fig. 5 gives the dimensionless frequency of the first symmetric mode. When $\gamma = \mu_0 = 0$, this frequency is equal to π^2. It greatly increases with self-weight. At fixed γ, it is observed that the frequency, which usually decays when heating, can indeed increase. This is due to the fact although N_0 continuously decays, the predeflection $|w_0|$ grows when heating and has a counteracting effect that tends to increase frequencies of symmetric modes.

Fig. 6 shows the frequency contour plots for the second symmetric and first antisymmetric modes. When $\gamma = \mu_0 = 0$, these frequencies are, respectively, equal to $9\pi^2$ and $4\pi^2$. For the self-weight parameter range used, the frequency of the 2nd symmetric mode never increases with temperature, which shows that the effect of w_0 on higher modes is far less pronounced than for the first one. As expected no frequency increase occurs for the antisymmetric mode either

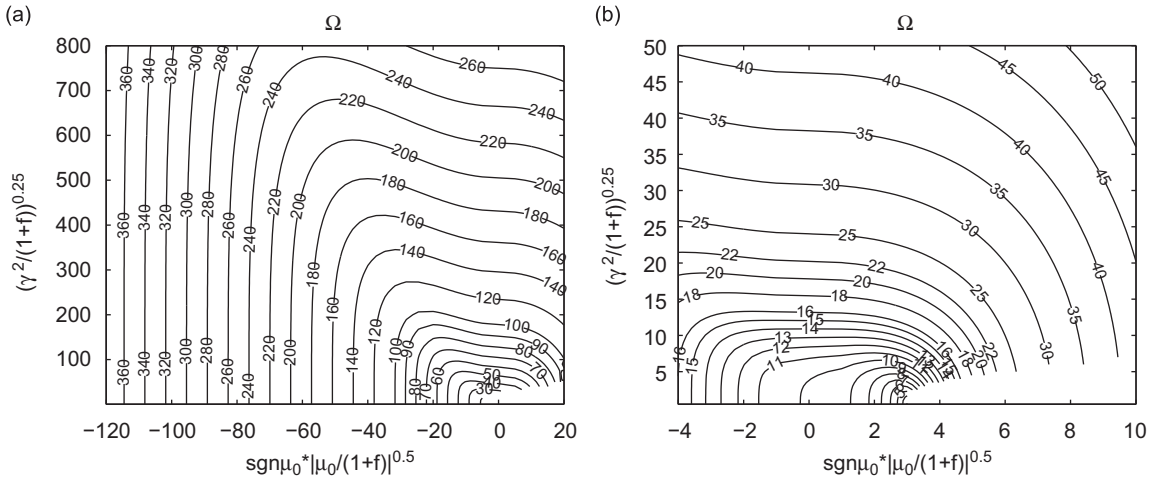

Fig. 5. Contour plot of the dimensionless frequency of the 1st symmetric mode (a) and its zoom (b) for $\kappa = \mu_1 = 0$.

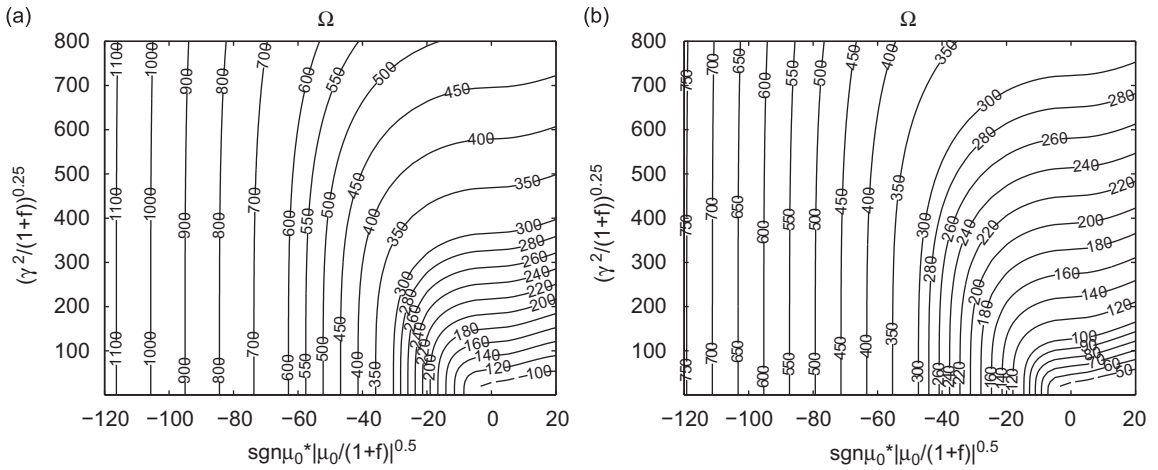

Fig. 6. Dimensionless frequency of the 2nd symmetric mode (a) and 1st antisymmetric mode (b) for $\kappa = \mu_1 = 0$.

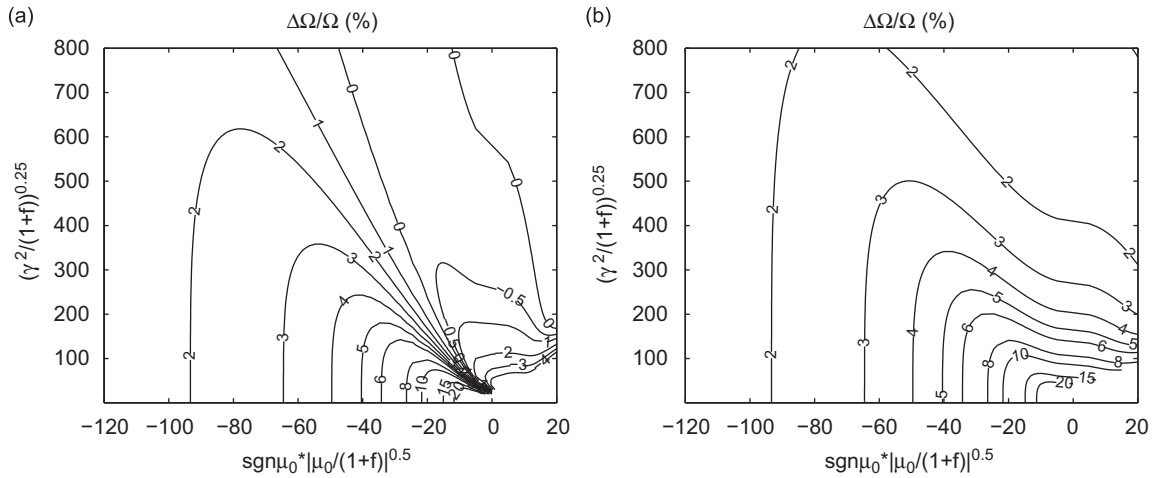

Fig. 7. Relative change of frequencies (in percent) between $\kappa = 1e3$ and $\kappa = 0$ for the first symmetric mode (a) and for the 1st antisymmetric mode (b) ($\mu_1 = 0$).

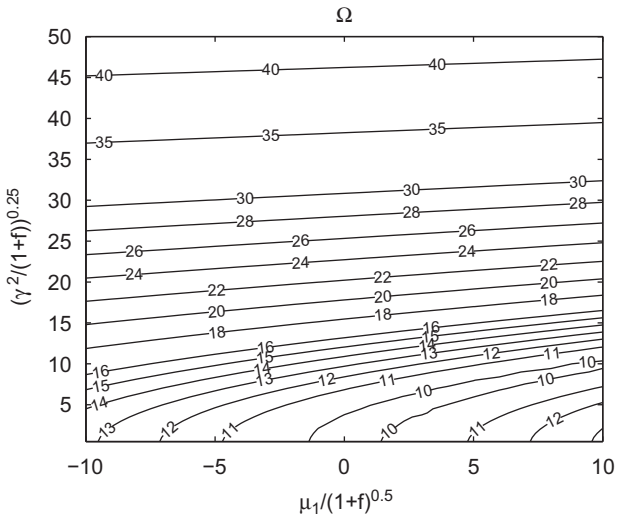

Fig. 8. Dimensionless frequency of the 1st symmetric mode for $\kappa = \mu_0 = 0$.

(antisymmetric modes being independent on $|w_0|$, as mentioned in Section 2.4.1). Note that given N_0, antisymmetric frequencies can be analytically determined from Eq. (15) when $\kappa = 0$, and are given by:

$$\Omega_n^a = 2n\pi\sqrt{4n^2\pi^2 + N_0} \tag{26}$$

The sensitivity of frequencies to boundary conditions is briefly studied by considering the extreme case of clamped ends ($\kappa \gg 1$). The plots for N_0 and $w_0(0)$ are not shown for conciseness. Fig. 7 gives contour plots for the relative change compared to frequencies obtained with simple supports ($\kappa = 0$). Boundary condition effects turn to be significant for lower values of γ and μ_0 (in the beam-like zone). The clamping effect tends to become greater for higher modes: the first antisymmetric mode, usually corresponding to the second natural frequency, is more sensitive than the first symmetric one. As a side remark concerning the 1st symmetric mode, one can note that there exists a zone where the frequency can become lower than with simple supports.

The effect of thermal bending moment on the 1st symmetric frequency is given by Fig. 8 for $\kappa = \mu_0 = 0$). This value of κ maximizes the effect of μ_1 (clamped beams are not affected by μ_1, as stated in Section 2.2). As explained in Section 3.1.1, positive values of μ_1 tend to decrease frequencies and inversely. It can be noted that the effect of thermal bending moment becomes negligible as the self-weight parameter increases (contour lines becomes horizontal). Also, its effect decreases and becomes negligible for higher modes (results not shown for conciseness).

By considering $\mu_{0_{eq}}+\mu_0$ instead of μ_0 in contour plots, Figs. 4–7 could also be used to obtain cable frequencies. However, the dimensionless parameters $\gamma^2/(1+f)$ and $\mu_0/(1+f)$ are far less convenient than Irvine parameters for the parametric study of cables, as done in the next subsection.

3.2. Cables

In this subsection, the proposed beam model is used for the study of cables, taking into account bending stiffness and temperature change. An external force H is hence initially prescribed at the end of the self-weighted beam. Thermal bending moments are neglected.

3.2.1. Validation

A first test concerns the effects of bending stiffness on cable frequencies without thermal loads. The proposed analytical solutions are compared to existing numerical results presented in Refs. [26,27] for four cables, having different values of sag and bending stiffness. Analytical frequencies found in Ref. [28] are also given. The cable characteristics are recalled in Table 1. Clamped supports are used. Table 2 shows the first two natural frequencies. Values obtained with the present theory agree with the results of literature. Only a slight discrepancy occurs for the 2nd frequency of Cable 2. In the present paper, it is emphasized that the prestressed state is calculated taking into account both bending stiffness and clamped conditions, as opposed to Refs. [26–28] where such effects are included for the dynamics only, which might explain small deviations.

For further insights, Table 2 also shows the results obtained from Irvine's theory as well as the proposed model with $\kappa=0$ (simple supports). It can be concluded that Irvine's theory is not applicable for Cables 3 and 4, their bending stiffness being not negligible ($\xi=50.5$). Also, bending stiffness mainly acts when boundary conditions are clamped.

A second test aims at evaluating the limitation of the model due to the assumption of small rotation, compared to Irvine's model for various sag-to-span ratio (without thermal load). One considers a high prescribed tension, $\xi=100$, in order to reduce the bending stiffness effects. The boundary conditions are simple supports ($\kappa=0$) with no flexibility ($f=0$). A constant safety factor $H/EA=1\text{e}{-3}$ is used. The slenderness ratio is then necessarily constant: $\sigma=\xi/\sqrt{H/EA}\simeq 3162$. The other cable characteristics are: $E=2.0\text{e}{+11}\,\text{Pa}$, $\rho=7800\,\text{kg m}^{-3}$, $g=9.81\,\text{m s}^{-2}$. Table 3 compares the sag-to-span and the frequency of the 1st symmetric mode obtained with the present model and with Irvine's theory. The length L is varying so that the sag-to-span ratio $w_0(0)/\sigma$ sweeps the range $[0.001;0.125]$ (0.125 is the limit of applicability of Irvine's solutions). λ^2 then varies from 0.064 to 887.6. Quite good agreement is found between both solutions, even for the highest sag-to-span ratio, which shows the validity of the proposed model for the study of cables.

Table 4 gives results when a temperature change $\Delta T=+40\,\text{K}$ is applied ($\alpha=1.2\text{e}{-5}\,\text{K}^{-1}$). One can note that the effect of temperature on frequencies diminishes as the sag-to-span increases. The proposed model is compared to the solution presented by the author in Ref. [29] (extension of Irvine's model to thermoelasticity). Both solutions are in good agreement, which ends the validation of the model for cables.

Table 1
Mechanical and geometric parameters of cables.

Cable	λ^2	ξ	ρA (kg/m)	g (N/kg)	L (m)	H (10^6 N)	E (Pa)	A (m^2)	I (m^4)
1	0.79	605.5	400.0	9.8	100.0	2.90360	1.5988e+10	7.8507e−3	4.9535e−6
2	50.70	302.7	400.0	9.8	100.0	0.72590	1.7186e+10	7.6110e−3	4.6097e−6
3	1.41	50.5	400.0	9.8	100.0	26.13254	2.0826e+13	7.8633e−3	4.9204e−6
4	50.70	50.5	400.0	9.8	100.0	0.72590	4.7834e+08	2.7345e−1	5.9506e−3

Table 2
Comparison of frequencies with literature ($\Delta T=0\,\text{K}$).

Mode	Cable 1		Cable 2		Cable 3		Cable 4	
	1st	2nd	1st	2nd	1st	2nd	1st	2nd
Finite difference [26]	0.440	0.853	0.428	0.464	1.399	2.679	0.447	0.464
Finite element [27]	0.441	0.854	0.421	0.460	1.400	2.682	0.438	0.461
Ricciardi [28]	0.441	0.855	0.429	0.463	1.400	2.682	0.447	0.465
Proposed model ($\kappa=1e3$)	0.441	0.855	0.429	0.468	1.393	2.682	0.447	0.460
Irvine [25]	0.440	0.852	0.426	0.463	1.350	2.556	0.426	0.463
Proposed model ($\kappa=0$)	0.440	0.852	0.426	0.468	1.352	2.576	0.429	0.470

Table 3
Comparison of results between the present theory and Irvine's model obtained for various sag-to-span ratios ($\Delta T = 0$ K).

	L (m)	20.91	209.1	418.2	627.3	1045	1673	2612
	λ^2	0.064	6.40	25.52	57.19	156.9	389.6	887.6
Irvine [25]	sag-to-span	0.001	0.01	0.02	0.03	0.05	0.08	0.125
	f_1^s (Hz)	3.839	0.472	0.332	0.288	0.210	0.135	0.087
Proposed model	sag-to-span	0.001	0.010	0.020	0.030	0.050	0.080	0.125
	f_1^s (Hz)	3.841	0.472	0.332	0.289	0.211	0.136	0.088

Table 4
Comparison of results between the present theory and Irvine's model obtained for various sag-to-span ratios ($\Delta T = +40$ K).

	L (m)	20.91	209.1	418.2	627.3	1045	1673	2612
	λ^2	0.064	6.40	25.52	57.19	156.9	389.6	887.6
	θ	0.480	0.480	0.479	0.479	0.477	0.472	0.462
Treyssede [29]	sag-to-span	0.002	0.014	0.023	0.032	0.052	0.081	0.126
	f_1^s (Hz)	2.829	0.496	0.355	0.297	0.207	0.134	0.087
Proposed model	sag-to-span	0.002	0.014	0.023	0.032	0.052	0.081	0.126
	f_1^s (Hz)	2.831	0.496	0.356	0.298	0.209	0.135	0.088

3.2.2. Parametric study

The combined effects of thermal loads and bending stiffness on cables are investigated for the following ranges of variation: $\lambda'^2 \in [1;200]$, $\theta' \in [-1;+1]$, $\xi \in [25;300]$. One considers clamped supports ($\kappa = 1e3, f = 0$), which maximizes the effects of bending stiffness.

In order to highlight bending stiffness effects without thermal stress, Fig. 9 first exhibits two-dimensional contour plots of $\Omega'/\pi = f(\lambda'^2, \xi)$ for the first antisymmetric mode and the first three symmetric modes. Frequencies tend towards asymptotic limits as the bending stiffness parameter increases, corresponding to Irvine's solutions. As opposed to antisymmetric modes, the influence of ξ on symmetric modes is strongly dependent on λ'^2. Generally, this influence tends to grow for higher values of λ'^2 and for higher modes. The same conclusions were already found in Refs. [27,28] and show the importance of taking into account bending stiffness in cable dynamics.

The effects of temperature can be quantified from two-dimensional contour plots of $\Delta\Omega/\Omega = f(\lambda'^2, \theta')$, where $\Delta\Omega/\Omega = \Omega(\lambda'^2, \theta')/\Omega(\lambda'^2, 0) - 1$ is the relative change in natural frequency under the influence of temperature. Fig. 10 plots the relative change of the 1st antisymmetric frequency for $\xi = 300$ and 50. For both values of ξ, the frequency sensitivity is slightly higher when cooling. For fixed values of θ', this sensitivity gradually becomes lower for cables having larger λ'^2. Note that comparing temperature sensitivity for different values of λ'^2 at fixed θ' implies that the ratio between the working stress H/A and Young's modulus E should remain almost constant. For a given cable material, comparisons for fixed θ' are hence indeed made for an almost constant safety factor, which is meaningful [29].

Concerning bending stiffness effects, the comparison of results in Fig. 10 between $\xi = 50$ and 300 shows that the difference of thermal relative change remains < 1 percent between $\xi = 50$ and 300: bending stiffness does not have a significant effect on the thermal behaviour of this frequency.

Fig. 11 plots the change of the 1st symmetric frequency for $\xi = 300$ and 50. Let us first consider the case $\xi = 300$. The thermal behaviour of this mode is strongly dependent on λ'^2 and quite different from Fig. 10. Roughly, the frequency relative change is rather small above $\log\lambda'^2 = 4.5$ ($\lambda'^2 \simeq 90$). Between 2.5 and 4.5 (λ'^2 between 12 and 90), it is more pronounced and the frequency is increasing with temperature. Below $\log\lambda'^2 = 2.5$ ($\lambda'^2 \simeq 12$), the behaviour changes again. For $\theta' < 0$ (cooling), the first frequency is increasing as the temperature is decreasing. However, for $\theta' > 0$ (heating), the modal behaviour is more complex: the frequency might increase or decrease depending on the value of λ'^2 as well as of θ'. The frequency might be not monotically varying with respect to temperature change, as it is the case for $\log\lambda'^2 = 2$ ($\lambda'^2 \simeq 7$) for instance (the frequency tends to increase for any negative or positive temperature change). As already explained for beam-like problems, the fact that the frequency can increase with temperature is due to the modification of sag (curvature increase, which counteracts the decrease of tension).

Unlike the first antisymmetric mode, the thermal relative change of Ω_1^s is strongly affected at $\xi = 50$. For instance at $\log\lambda'^2 = 4.5$ ($\lambda'^2 \simeq 90$) and $\theta' = +1$, the relative change due to temperature is 0 percent for $\xi = 300$ and 5 percent for $\xi = 50$. The action of bending stiffness combined with thermal change is hence clearly non-negligible.

Fig. 12 plots the change of the 2nd symmetric frequency for $\xi = 300$ and 50. The effect of bending stiffness upon this mode is also significant (differences of several percents exist between both ξ). However, the thermal behaviour of the 3rd symmetric mode is quite less affected at $\xi = 50$ (Fig. 13), which tends to show that the bending stiffness influence on

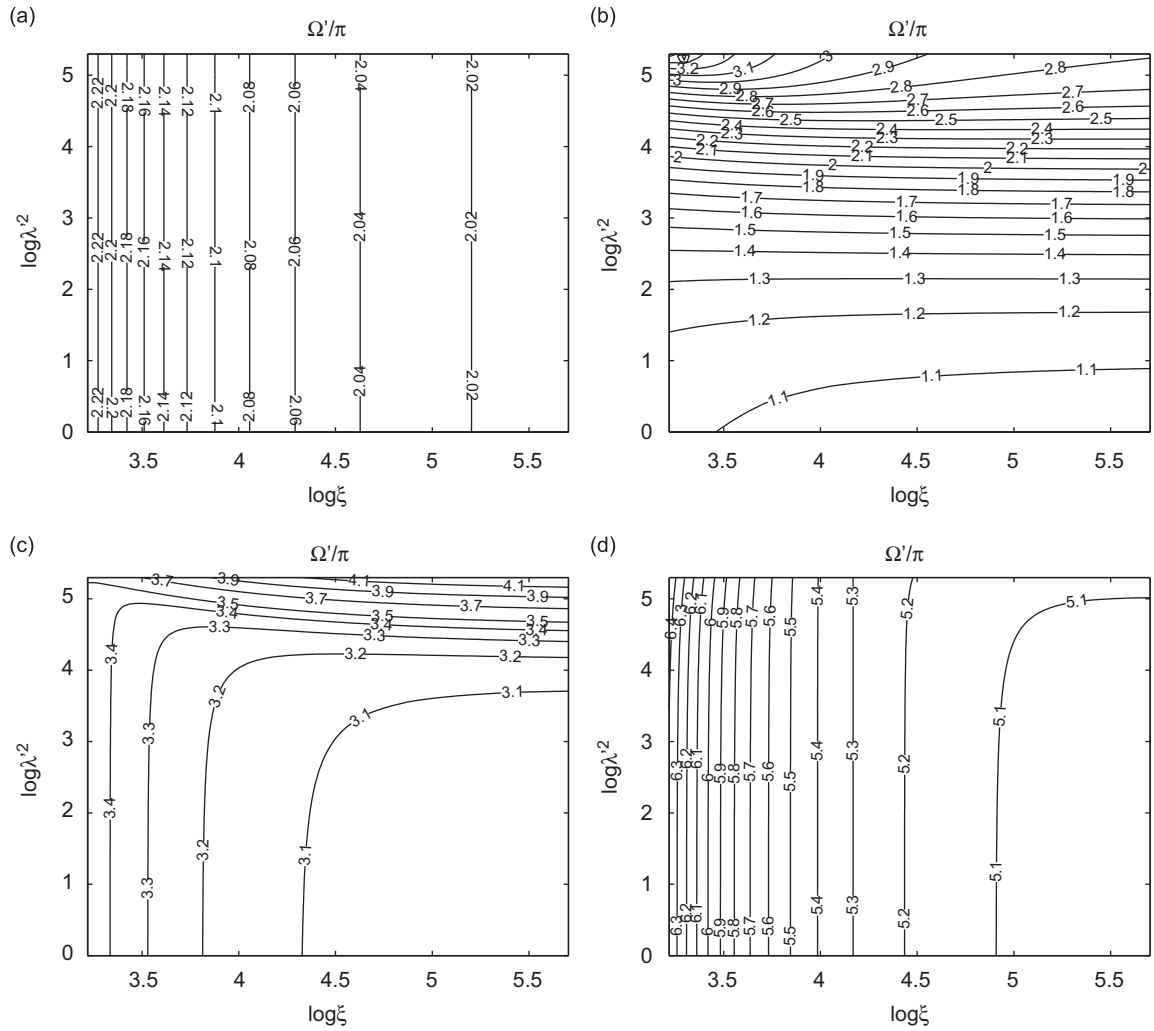

Fig. 9. Natural frequencies as a function of ξ and λ'^2 for the first antisymmetric (a), first symmetric (b), second symmetric (c) and third symmetric modes (d) ($\theta' = 0$).

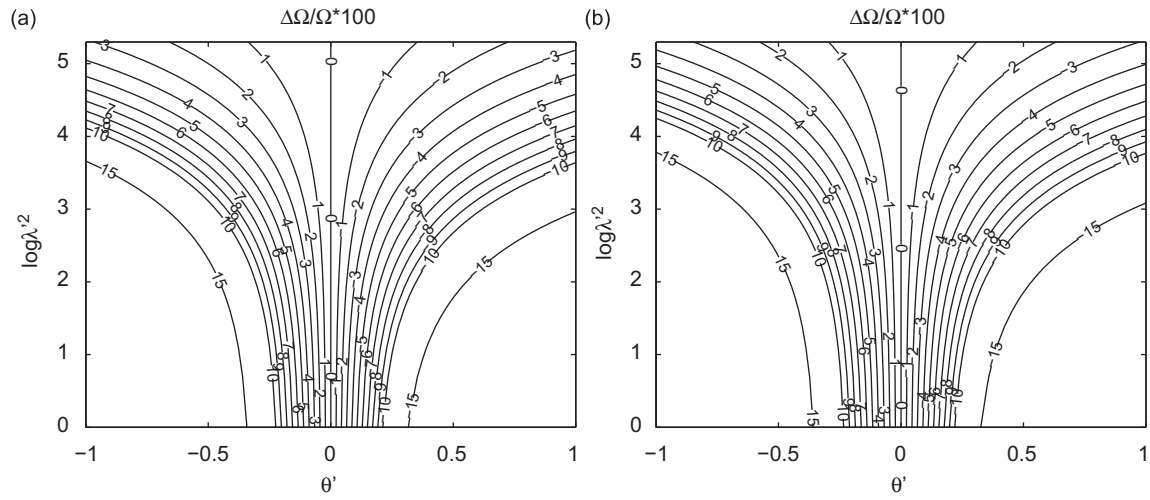

Fig. 10. Relative change in natural frequency ($\times 100$) of the 1st antisymmetric mode for $\xi = 300$ (a) and $\xi = 50$ (b).

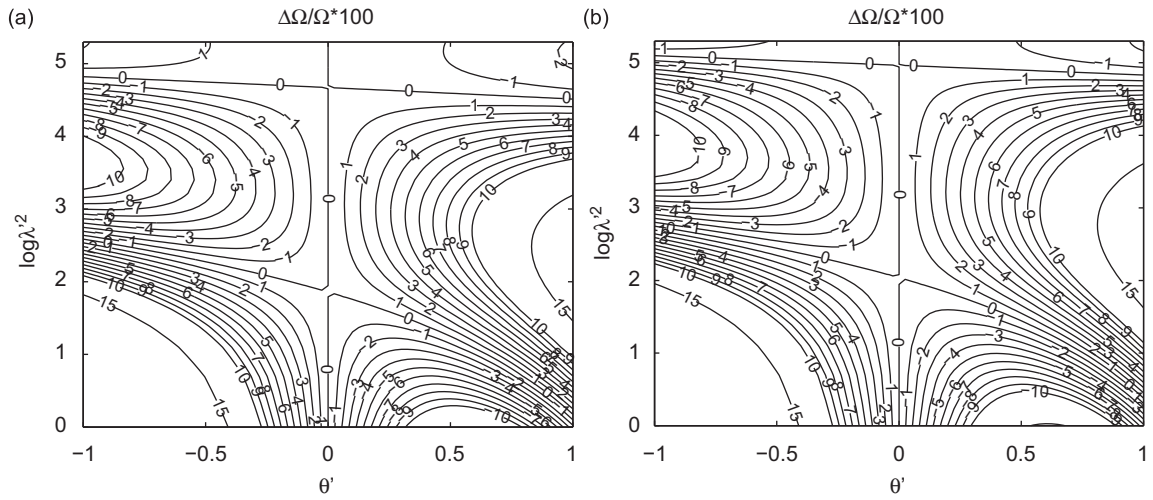

Fig. 11. Relative change in natural frequency (×100) of the 1st symmetric mode for $\xi = 300$ (a) and $\xi = 50$ (b).

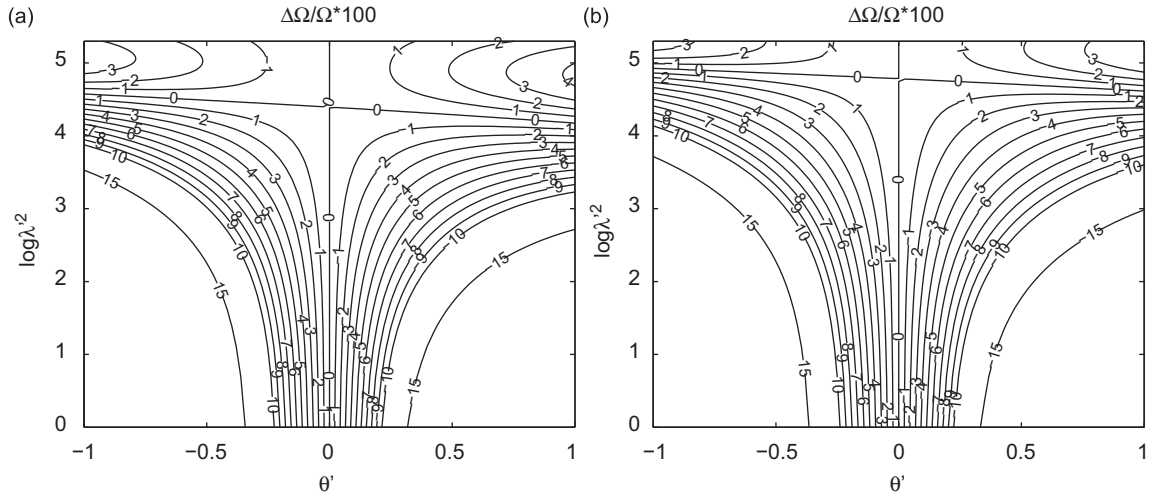

Fig. 12. Relative change in natural frequency (×100) of the 2nd symmetric mode for $\xi = 300$ (a) and $\xi = 50$ (b).

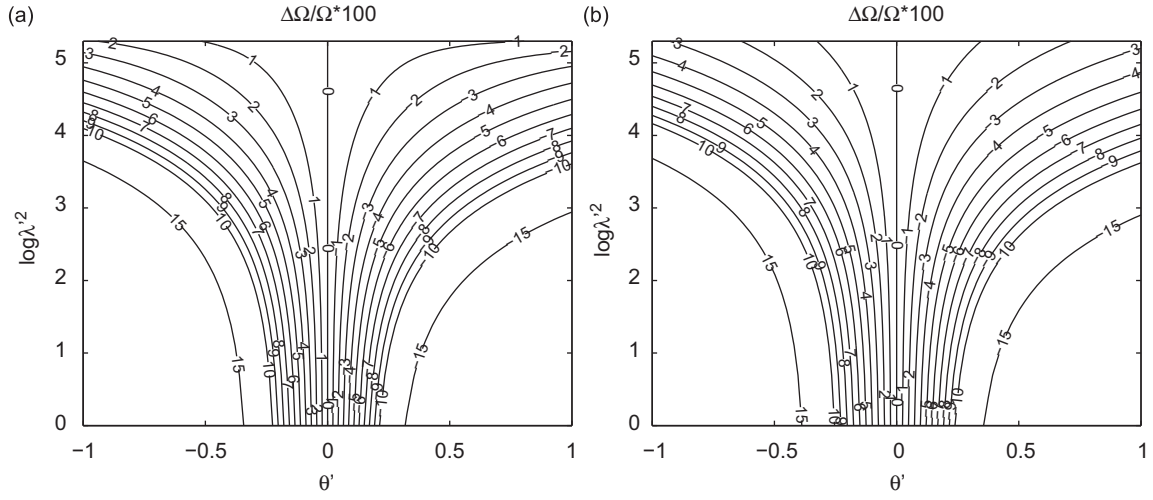

Fig. 13. Relative change in natural frequency (×100) of the 3rd symmetric mode for $\xi = 300$ (a) and $\xi = 50$ (b).

thermal relative change of frequencies decays for higher modes. It can also be noticed that as the mode order increases, the thermal behaviour becomes identical to that of antisymmetric modes (compare Fig. 10 with 13), due to the fact that higher modes are less sensitive to predisplacement (as already noticed for beams).

As a final remark, results obtained in Figs. 10–13 for $\xi = 300$ coincide with the ones found in Ref. [29] with neglected bending stiffness.

4. Conclusion

A unified analytical model has been proposed to investigate the effects of temperature on the modal behaviour of horizontal beams taking into account self-weight, and cables taking into account bending stiffness. Various boundary conditions can be considered thanks to the introduction of axial and torsional springs. Solutions are valid for small rotations. For cables, the sag-to-span ratio must remain small (typically $< \frac{1}{8}$ as in Irvine's theory). Dimensionless parameters governing equilibrium equations have been highlighted. For beams, it has been shown that the number of independent parameters is reduced to four. These parameters are, respectively, associated with the self-weight, thermal force, thermal bending moment and torsional spring. A fifth parameter related to the prescribed force is introduced for cable-like problems, corresponding to the so-called bending stiffness parameter ξ. Some modified Irvine parameters have been proposed in this paper, allowing a precise characterization of cables with bending stiffness.

For beam problems, the model has been validated thanks to FE solutions and a parametric study has been briefly conducted in order to highlight the combined effects of thermal loads and self-weight on natural frequencies. For cable problems, solutions have been compared with existing results in the literature obtained without thermal effects or bending stiffness. A parametric study combining the effects of sag-extensibility, thermal change and bending stiffness has been briefly performed. It has been found that the effect of bending stiffness on the thermal relative change of frequencies can be important.

Results show that the thermal loads due to climatic variations can have a significant effect on the natural frequencies of slender beams and cables. Under self-weight, frequencies have a complex thermal behaviour, which may be nonlinearly and non-monotically varying with respect to temperature. The thermoelastic behaviour of civil structures is hence likely to affect the robustness of vibration based methods in SHM.

Appendix A. Note on heat transfer

As assumed through the whole paper, the temperature does not vary along x. For simplicity, let us also assume that it also remains constant along y. The problem is reduced on the transverse direction z of the beam. The physics of heat transfer being different from that of beam mechanics, z^* and t^* are made dimensionless with some different characteristic length and time, denoted e and t_c' . e is typically chosen as half the thickness and t_c' must be representative of the heat process (roughly, one day for climatic variations).

k, C and h will, respectively, denote the thermal conductivity, specific heat capacity and convection heat transfer coefficient. q_v and q_s will be the time of rate of heat generated per unit volume (for instance, due to the hydration reaction of cement for concrete structures) and time rate of heat transfer per unit area on the boundary (due to solar radiation for instance).

Heat transfers in beams are governed by the differential equation [48]:

$$\dot{T} - \mathrm{Fo}\frac{\mathrm{d}^2 T}{\mathrm{d}z^2} = \phi - \beta T_{\mathrm{ref}}\dot{\varepsilon} \tag{27}$$

and its associated boundary condition:

$$\pm \frac{\mathrm{d}T}{\mathrm{d}z} + \mathrm{Bi}(T - T_\infty)\Big|_{\pm 1/2} = \varphi \tag{28}$$

where T_∞ is the air temperature and ε is the axial strain of the beam. Dimensionless parameters are defined as: $\mathrm{Fo} = kt_c'/\rho C e^2$ (Fourier number), $\mathrm{Bi} = he/k$ (Biot number), $\beta = E\alpha/\rho C$ (thermomechanical coupling parameter), $\phi = q_v t_c'/\rho C$ and $\varphi = q_s e/k$.

For standard civil materials (concrete, steel), $\beta \sim 1$ so that the last term of Eq. (27) can be neglected thanks to the assumption of small strain. This *a priori* justify the usual assumption that heat transfer equilibrium equations are not coupled to mechanics (throughout this paper, the temperature is considered as known). When $\mathrm{Fo} \gg 1$, the heat process can be considered as stationary. When Bi is small enough, the temperature can be considered as constant on the cross-section.

Let us consider a civil structure made of standard concrete and subjected to climatic thermal changes: $E = 30\,\mathrm{GPa}$, $\alpha = 1e{-}5\,\mathrm{K}^{-1}$, $\rho = 2400\,\mathrm{kg\,m}^{-3}$, $C = 850\,\mathrm{J\,kg}^{-1}\,\mathrm{K}^{-1}$, $k = 2\,\mathrm{W\,m}^{-1}\,\mathrm{K}^{-1}$, $h = 20\,\mathrm{W\,m}^{-2}\,\mathrm{K}^{-1}$, $t_c' = 43\,200\,\mathrm{s}$ (12 h). This yields $\mathrm{Fo} = 0.042/e^2$ and $\mathrm{Bi} = 10e$. For large civil structures such as bridge decks, e is $> 1\,\mathrm{m}$ so that, generally:

- the evolution of temperature cannot be considered as stationary;
- the temperature does not remain spatially constant on the beam cross-section (thermal bending moment cannot be *a priori* neglected);

- the mechanical evolution of a thermally prestressed state is quasi-static, provided that for climatic change, the heat characteristic time t_c' is far greater than the mechanical characteristic time t_c.

For cables made of steel, one has: $E=200\,\mathrm{GPa}$, $\alpha=1.2e{-}5\,\mathrm{K}^{-1}$, $\rho=7800\,\mathrm{kg\,m}^{-3}$, $C=500\,\mathrm{J\,kg}^{-1}\,\mathrm{K}^{-1}$, $k=20\,\mathrm{W\,m}^{-1}\,\mathrm{K}^{-1}$, so that $\mathrm{Fo}=0.22/e^2$ and $\mathrm{Bi}=e$. e is generally small enough for the temperature to be considered as almost uniform on the cable cross-section (but the heat process cannot be considered as stationary).

These remarks justify assumptions used in this paper. Examples of heat transfer analyses and thermomechanical effects applied to civil structures can be found in Refs. [49–51] for instance.

Appendix B. Expressions of α_- and α_+

The expressions of α_- and α_+ are, respectively, given as:

$$\alpha_- = \frac{\dfrac{\gamma}{N_0}\left(\cos\dfrac{\lambda_-}{2}-\dfrac{2\sin\dfrac{\lambda_-}{2}}{\lambda_-}\right)+\dfrac{2B_0\lambda_-N_0}{N_0+\lambda_-^2}\left(\lambda_-\cos\dfrac{\lambda_-}{2}\dfrac{\sinh\dfrac{\sqrt{N_0}}{2}}{\sqrt{N_0}}-\sin\dfrac{\lambda_-}{2}\cosh\dfrac{\sqrt{N_0}}{2}\right)}{(1+f)\Omega^2+B_0\gamma\left(\cosh\dfrac{\sqrt{N_0}}{2}-2\dfrac{\sinh\dfrac{\sqrt{N_0}}{2}}{\sqrt{N_0}}\right)-\dfrac{B_0^2N_0^2}{2}\left(1-\dfrac{\sinh\sqrt{N_0}}{\sqrt{N_0}}\right)} \tag{29}$$

and:

$$\alpha_+ = \frac{\dfrac{\gamma}{N_0}\left(\cosh\dfrac{\lambda_+}{2}-2\dfrac{\sinh\dfrac{\lambda_+}{2}}{\lambda_+}\right)-\dfrac{2B_0\lambda_+N_0}{N_0-\lambda_+^2}\left(\lambda_+\cosh\dfrac{\lambda_+}{2}\dfrac{\sinh\dfrac{\sqrt{N_0}}{2}}{\sqrt{N_0}}-\sinh\dfrac{\lambda_+}{2}\cosh\dfrac{\sqrt{N_0}}{2}\right)}{(1+f)\Omega^2+B_0\gamma\left(\cosh\dfrac{\sqrt{N_0}}{2}-2\dfrac{\sinh\dfrac{\sqrt{N_0}}{2}}{\sqrt{N_0}}\right)-\dfrac{B_0^2N_0^2}{2}\left(1-\dfrac{\sinh\sqrt{N_0}}{\sqrt{N_0}}\right)} \tag{30}$$

References

[1] A. Bokaian, Natural frequencies of beams under compressive axial loads, *Journal of Sound and Vibration* 126 (1988) 49–65.
[2] H. Abramovich, Natural frequencies of Timoshenko beams under compressive axial loads, *Journal of Sound and Vibration* 157 (1992) 183–189.
[3] N. Ganesan, V. Pradeep, Buckling and vibration of sandwich beams with viscoelastic core under thermal environments, *Journal of Sound and Vibration* 286 (2005) 1067–1074.
[4] V. Pradeep, N. Ganesan, K. Bhaskar, Vibration and thermal buckling of composite sandwich beams with viscoelastic core, *Composite Structures* 81 (2007) 60–69.
[5] Sharnappa, N. Ganesan, R. Sethuraman, Dynamic modeling of active constrained layer damping of composite beam under thermal environment, *Journal of Sound and Vibration* 305 (2007) 728–749.
[6] H.J. Xiang, J. Yang, Free and forced vibration of a laminated FGM Timoshenko beam of variable thickness under heat conduction, *Composites Part B—Engineering* 39 (2008) 292–303.
[7] T. Yokoyama, Vibrations of a hanging Timoshenko beam under gravity, *Journal of Sound and Vibration* 141 (1990) 245–258.
[8] H. Abramovich, Free-vibrations of gravity loaded composite beams, *Composite Structures* 23 (1993) 17–26.
[9] L.N. Virgin, S.T. Santillan, D.B. Holland, Effect of gravity on the vibration of vertical cantilevers, *Mechanics Research Communications* 34 (2007) 312–317.
[10] J.W. Hijmissen, W.T. van Horssen, On transverse vibrations of a vertical Timoshenko beam, *Journal of Sound and Vibration* 314 (2008) 161–179.
[11] H. Lurie, Lateral vibrations as related to structural stability, *Journal of Applied Mechanics* 19 (1952) 195–204.
[12] R.L. Bisplinghoff, T.H.H. Pian, On the vibrations of thermally buckled bars and plates, *Ninth International Congress for Applied Mechanics* 7 (1956) 307–318.
[13] S.M. Dickinson, Lateral vibration of slightly bent slender beams subject to prescribed axial end displacement, *Journal of Sound and Vibration* 68 (1980) 507–514.
[14] C.S. Kim, S.M. Dickinson, The flexural vibration of slightly curved slender beams subject to axial end displacement, *Journal of Sound and Vibration* 104 (1986) 170–175.
[15] N. Yamaki, A. Mori, Non-linear vibrations of a clamped beam with initial deflection and initial axial displacement: 1. Theory, *Journal of Sound and Vibration* 71 (1980) 333–346.
[16] N.C. Perkins, Planar vibration of an elastica arch—theory and experiment, *Journal of Vibration and Acoustics—Transactions of the Asme* 112 (1990) 374–379.
[17] A.H. Nayfeh, W. Kreider, T.J. Anderson, Investigation of natural frequencies and mode shapes of buckled beams, *AIAA Journal* 33 (1995) 1121–1126.
[18] D. Addessi, W. Lacarbonara, A. Paolone, On the linear normal modes of planar pre-stressed curved beams, *Journal of Sound and Vibration* 284 (2005) 1075–1097.
[19] R.H. Plaut, J.E. Sidbury, L.N. Virgin, Analysis of buckled and pre-bent fixed-end columns used as vibration isolators, *Journal of Sound and Vibration* 283 (2005) 1216–1228.
[20] O. Paul, H. Baltes, Mechanical behavior and sound generation efficiency of prestressed, elastically clamped and thermomechanically driven thin film sandwiches, *Journal of Micromechanics and Microengineering* 9 (1999) 19–29.
[21] S.R. Li, Z.C. Teng, Y.H. Zhou, Free vibration of heated Euler–Bernoulli beams with thermal postbuckling deformations, *Journal of Thermal Stresses* 27 (2004) 843–856.
[22] F. Treyssède, Prebending effects upon the vibrational modes of thermally prestressed planar beams, *Journal of Sound and Vibration* 307 (2007) 295–311.

[23] M.H. Ghayesh, S.E. Khadem, Rotary inertia and temperature effects on non-linear vibration, steady-state response and stability of an axially moving beam with time-dependent velocity, *International Journal of Mechanical Sciences* 50 (2008) 389–404.
[24] L.N. Virgin, R.H. Plaut, Post-buckling and vibration of linearly elastic and softening columns under self-weight, *International Journal of Solids and Structures* 41 (2004) 4989–5001.
[25] H.M. Irvine, *Cable Structures*, The MIT Press, Cambridge, New Jersey, 1981.
[26] A.B. Mehrabi, H. Tabatabai, Unified finite difference formulation for free vibration of cables, *Journal of Structural Engineering* 124 (1998) 1313–1322.
[27] Y.Q. Ni, J.M. Ko, G. Zheng, Dynamic analysis of large-diameter sagged cables taking into account flexural rigidity, *Journal of Sound and Vibration* 257 (2002) 301–319.
[28] G. Ricciardi, F. Saitta, A continuous vibration analysis model for cables with sag and bending stiffness, *Engineering Structures* 30 (2008) 1459–1472.
[29] F. Treyssède, Free linear vibrations of cables under thermal stress, *Journal of Sound and Vibration* 327 (2009) 1–8.
[30] H. Sohn, M. Dzwonczyk, E.G. Straser, A.S. Kiremidjian, K.H. Law, T. Meng, An experimental study of temperature effect on modal parameters of the Alamosa Canyon Bridge, *Earthquake Engineering & Structural Dynamics* 28 (1999) 879–897.
[31] B. Peeters, G. De Roeck, One-year monitoring of the z24-bridge: environmental effects versus damage events, *Earthquake Engineering & Structural Dynamics* 30 (2001) 149–171.
[32] A. Teughels, G. De Roeck, Structural damage identification of the highway bridge z24 by fe model updating, *Journal of Sound and Vibration* 278 (2004) 589–610.
[33] J.T. Kim, J.H. Park, B.J. Lee, Vibration-based damage monitoring in model plate-girder bridges under uncertain temperature conditions, *Engineering Structures* 29 (2007) 1354–1365.
[34] N. Bouaanani, Numerical investigation of the modal sensitivity of suspended cables with localized damage, *Journal of Sound and Vibration* 292 (2006) 1015–1030.
[35] M. Lepidi, V. Gattulli, F. Vestroni, Static and dynamic response of elastic suspended cables with damage, *International Journal of Solids and Structures* 44 (2007) 8194–8212.
[36] T. Livingston, J.G. Beliveau, D.R. Huston, Estimation of axial load in prismatic members using flexural vibrations, *Journal of Sound and Vibration* 179 (1995) 899–908.
[37] W.X. Ren, G. Chen, W.H. Hu, Empirical formulas to estimate cable tension by cable fundamental frequency, *Structural Engineering and Mechanics* 20 (2005) 363–380.
[38] B.H. Kim, T. Park, Estimation of cable tension force using the frequency-based system identification method, *Journal of Sound and Vibration* 304 (2007) 660–676.
[39] B. Peeters, J. Maeck, G. De Roeck, Vibration-based damage detection in civil engineering: excitation sources and temperature effects, *Smart Materials & Structures* 10 (2001) 518–527.
[40] E. Balmes, M. Basseville, F. Bourquin, L. Mevel, H. Nasser, F. Treyssède, Merging sensor data from multiple temperature scenarios for vibration monitoring of civil structures, *Structural Health Monitoring—An International Journal* 7 (2008) 129–142.
[41] A. Deraemaeker, E. Reynders, G. De Roeck, J. Kullaa, Vibration-based structural health monitoring using output-only measurements under changing environment, *Mechanical Systems and Signal Processing* 22 (2008) 34–56.
[42] R.G. Rohrmann, M. Baessler, S. Said, W. Schmid, W. F. Ruecker, Sem, Structural causes of temperature affected modal data of civil structures obtained by long time monitoring, Imac-Xviii: a Conference on Structural Dynamics (San Antonio), Vols. 1 and 2, Proceedings 4062, 2000, pp. 1–7.
[43] K. Kanazawa, Structural damage detection from natural frequency eliminated by temperature effect, *Proceedings of the International Modal Analysis Conference* (*IMAC*), St. Louis, USA, 2006.
[44] A. Baz, Robust control of active constrained layer damping, *Journal of Sound and Vibration* 211 (1998) 467–480.
[45] S.S. Na, L. Librescu, H.D. Jung, Dynamics and active bending vibration control of turbomachinery rotating blades featuring temperature-dependent material properties, *Journal of Thermal Stresses* 27 (2004) 625–644.
[46] M. Parisse, F. Curti, D. De Rosa, Dynamic response of a system driven by thermal actuation, *Spaceflight Mechanics* 2004 (119) (2005) 821–832.
[47] B.A. Boley, J.H. Wiener, *Theory of Thermal Stresses*, Dover, New York, 1997.
[48] E. Manoach, P. Ribeiro, Coupled thermoelastic large amplitude vibrations of Timoshenko beams, *International Journal of Mechanical Sciences* 46 (2004) 1589–1606.
[49] A. Saetta, R. Scotta, R. Vitaliani, Stress-analysis of concrete structures subjected to variable thermal loads, *Journal of Structural Engineering—ASCE* 121 (1995) 446–457.
[50] M. Tong, L.G. Tham, F.T.K. Au, P.K.K. Lee, Numerical modelling for temperature distribution in steel bridges, *Computers & Structures* 79 (2001) 583–593.
[51] A. Dwivedi, P. Bhargava, N. Bhandari, Effect of non-linear temperature distributions in concrete box girder bridges, *Journal of Structural Engineering (Madras)* 32 (2006) 421–430.